Predicted phase diagram of boron-carbon-nitrogen

Hantao Zhang
School of the Gifted Young, University of Science and Technology of China, Hefei, Anhui, China 230026

Sanxi Yao and Michael Widom
Department of Physics, Carnegie Mellon University, Pittsburgh, Pennsylvania 15213, USA
(Received 24 December 2015; revised manuscript received 21 March 2016; published 8 April 2016)

Noting the structural relationships between phases of carbon and boron carbide with phases of boron nitride and boron subnitride, we investigate their mutual solubilities using a combination of first-principles total energies supplemented with statistical mechanics to address finite temperatures. Thus we predict the solid-state phase diagram of boron-carbon-nitrogen (B-C-N). Owing to the large energy costs of substitution, we find that the mutual solubilities of the ultrahard materials diamond and cubic boron nitride are negligible, and the same for the quasi-two-dimensional materials graphite and hexagonal boron nitride. In contrast, we find a continuous range of solubility connecting boron carbide to boron subnitride at elevated temperatures. An electron-precise ternary compound $B_{13}CN$ consisting of B_{12} icosahedra with NBC chains is found to be stable at all temperatures up to melting. It exhibits an order-disorder transition in the orientation of NBC chains at approximately $T = 500$ K. We also propose that the recently discovered binary $B_{13}N_2$ actually has composition $B_{12.67}N_2$.

DOI: 10.1103/PhysRevB.93.144107

I. INTRODUCTION

Elemental boron and its compounds exhibit interesting and complex structures, many of which feature icosahedral clusters of boron atoms and many of which remain imprecisely known [1–3]. Here we explore compounds of boron with carbon and nitrogen. These three elements occupy adjacent positions in the periodic table, exhibiting similar small size and covalent bonding ability, while differing in their valences. We model and predict the solid-state binary phase diagrams of B-C and B-N, and the B-C-N ternary. Interestingly, several of the elemental and binary structures are shared in common, so we explore their mutual solubilities. In doing so, we discover a ternary that we predict to be stable.

The common structure types are diamond and cubic boron nitride (both are fcc with two-atom primitive cells), graphite and hexagonal boron nitride (both are stacked honeycomb lattices; graphite has the Bernal AB stacking, while *h*-BN is Aa), and boron carbide and boron subnitride [4] (both have rhombohedral cells containing a 12-atom icosahedron and a three-atom chain). Diamond and *c*-BN are both ultrahard materials [5–8], as are boron carbide and boron subnitride. Graphite and *h*-BN can exist as isolated single-atom thick layers forming exotic two-dimensional materials [9].

Diamond converts into *c*-BN and graphite converts into *h*-BN through the isoelectronic replacement of C_2 with BN, thus preserving their optimal bonding characteristics. However, the conversion of boron carbide (nominally $B_{13}C_2$ but sometimes denoted B_4C) into boron subnitride (nominally $B_{13}N_2$) fails to preserve electron counts. Neither $B_{13}C_2$ nor $B_{13}N_2$ yield electron-precise bonding and this plays an important role in our following analysis, which exploits partial occupancy and substitutional disorder.

The following sections summarize the existing knowledge of structural stability in the B-C-N alloy system. Then we outline our theoretical methods that include first-principles total-energy calculation, electron counting analysis, and statistical mechanics. Our main results follow. Briefly, in the diamond/*c*-BN and in the graphite/*h*-BN structures, we demonstrate negligible mutual solubilities; in the icosahedron-based structures, we revise the stoichiometry of boron subnitride from $B_{13}N_2$ to $B_{12.67}N_2$, and we propose continuous solubility from boron carbide to boron subnitride above $T = 1355$ K. Finally, we predict stability at all temperatures up to melting of a ternary, $B_{13}CN$.

A. Elemental B, C, and N

Elemental boron exists in multiple allotropes [1]: α-B, consisting of a rhombohedral lattice of B_{12} icosahedra, is stable at high pressures and low temperatures; β-B, with a primitive cell of more than 105 atoms and a proliferation of partially occupied sites, is stable at high temperature and low pressures. The precise $\alpha - \beta$ boundary is not known experimentally at low temperature and pressure, though density functional theory (DFT) total energies suggest that β is the ground state at $T = 0$ K and $P = 0$ [3,10]. Elemental carbon takes the graphite structure at low pressure, which is a Bernal (AB) stacking of carbon honeycomb (i.e., graphene) lattices. At high pressure, above a few GPa, it transforms to diamond, which can be described as a pair of interpenetrating fcc lattices. Elemental nitrogen forms an N_2 molecular gas under ambient conditions. At low temperature, it crystallizes into a cubic form with four N_2 molecules per cell.

B. Binary B-C, B-N, and C-N

The B-C binary phase diagram [11] exhibits a single-phase boron carbide at ambient pressure. The underlying structure is well established, consisting of a rhombohedral cell with a 12-atom icosahedron and a three-atom chain comprising 15 atomic sites per cell (see Fig. 1). What is not well established is the distribution of B and C atoms among these sites, as the icosahedron can support composition B_{12}, $B_{11}C$, and $B_{10}C_2$, while the chain can be CBC, BBC, B_4, or even possess vacancies [12–15]. Substitutional disorder leads to

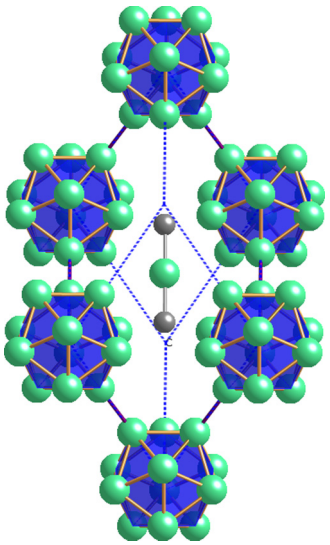

FIG. 1. Cutaway view of idealized boron carbide structure. The primitive cell is a rhombohedron with a B_{12} icosahedron on each vertex and a three-atom CBC chain along the rhombohedral axis. Intericosahedral bonds along rhombohedron edges connect boron atoms at *polar* sites. Boron atoms at *equatorial* sites bond to the chain carbon atoms. Icosahedra at two vertices have been removed for visual clarity.

variable composition, ranging from 9% to 19.2% carbon. The high-temperature solid solution should resolve into one or a few phases of precise stoichiometry at low temperature [16]. Density functional theory predicts *two* phases, B_{12}·CBC and $B_{11}C$·CBC, in a notation that specifies the icosahedron followed by the chain [17–20]. Other possibilities [21] are $B_{11}C$·CC and $B_{11}C$·C-C (- means vacancy), which are even richer in C, but are metastable with respect to B_4C.

The B-N binary phase diagram [22,23] contains a single phase, *h*-BN, at ambient pressure. The structure is an Aa stacking of BN honeycomb lattices, with B and N swapping positions in alternate layers [24], although other stacking types have been reported [25]. At $P = 5$ GPa, *c*-BN replaces *h*-BN as the low-temperature structure, and an additional phase $B_{13}N_2$ is reportedly synthesized at high temperature but remains stable at low temperature [26]. The Rietveld refinement claims the structure is B_{12}·NBN, with all sites fully occupied [4].

Binary C-N compounds such as C_3N_4 and $C_{11}N_4$ have been proposed theoretically [27,28] on the basis of isoelectronic substitutions of nitrogen and vacancies. Cubic variants are expected to be superhard, such as diamond, while graphitic variants are expected to be energetically more stable [29,30]. While cubic forms have been produced mostly in thin-film or nanocrystalline forms [31], macroscopic flakes of graphitic carbon nitride have recently been produced [32].

C. Boron carbon nitrogen ternary

Little experimental data exist on the B-C-N ternary. Previous phase diagrams are either presented at very high temperature or lack detailed information, especially at the high boron corner [33]. No stable compounds have been reported in the B-C-N ternary system. However, variants of diamond/*c*-BN such as BC_2N and BC_4N have been suggested theoretically [34–36] or synthesized experimentally [37,38] at high temperatures and pressures. Among layered and two-dimensional (2D) materials, there is controversy over whether C can substitute into *h*-BN, and vice versa. Some reports find that C and *h*-BN segregate [39], whereas others report B-C-N ternary alloys [40–42]. This miscibility may depend on temperature [43,44] and may involve filling some honeycomb cells [45].

II. METHODS

A. First-principles enthalpies

We use VASP [46–49] with projector augmented wave (PAW) [50,51] potentials to calculate total energies within the Perdew-Burke-Ernzerhof (PBE) [52] density functional approximation. Internal coordinates and lattice parameters are fully relaxed, and the *k*-point mesh density is increased until energies converge to within 1 meV/atom. We keep the plane-wave energy cutoff at 400 eV for all structures and employ a Fermi-level smearing of 0.2 eV, except for elemental N, which requires 0.05 eV. Periodic boundary conditions are utilized in all cases.

Relaxed total energy E is the enthalpy at $T = 0$ K and $P = 0$. For calculations under pressure, we take $H = E + PV$. Usually we consider the enthalpy of formation ΔH, defined as the enthalpy per atom relative to a tie line or tie plane connecting the enthalpies of pure elements in their stable forms. Given a set of compositions and enthalpies of plausible structures, the convex hull of this set predicts the $T = 0$ K phase diagram. Specifically, convex hull vertices predict the pure phases, while tie lines or tie planes connecting the vertices correspond to the coexistence of pure phases. We also define the *relative* enthalpy of formation for metastable structures, $\Delta\Delta H$, which is the enthalpy relative to the convex hull at the same composition. Figure 2 illustrates our predicted convex hull for B-C-N.

B. Electron counting

Molecular orbital theory provides a convenient way to analyze chemical bonding, and in turn to anticipate the relative stability of structures and compounds. In general, completely filling all bonding orbitals results in the greatest degree of stability. Incompletely filling bonding states leaves a structure at risk of losing stability to an alternative with filled bonding states, while filling an antibonding state can be strongly destabilizing.

In cubic structures such as diamond and *c*-BN, each atom has four near neighbors in a tetrahedral arrangement. Hybrid sp^3 orbitals form covalent σ bonds between neighbors, and these bonding states fill completely if the mean valence of the atoms is 4. In layered honeycomb structures such as graphite and *h*-BN, each atom has three near neighbors in-plane. Hybrid sp^2 orbitals form in-plane σ bonds utilizing three electrons per atom, while the remaining p_z orbitals completely fill the bonding states of the itinerant π band up to the Dirac point. Hence, diamond, *c*-BN, graphite, and *h*-BN can all be regarded as "electron precise."

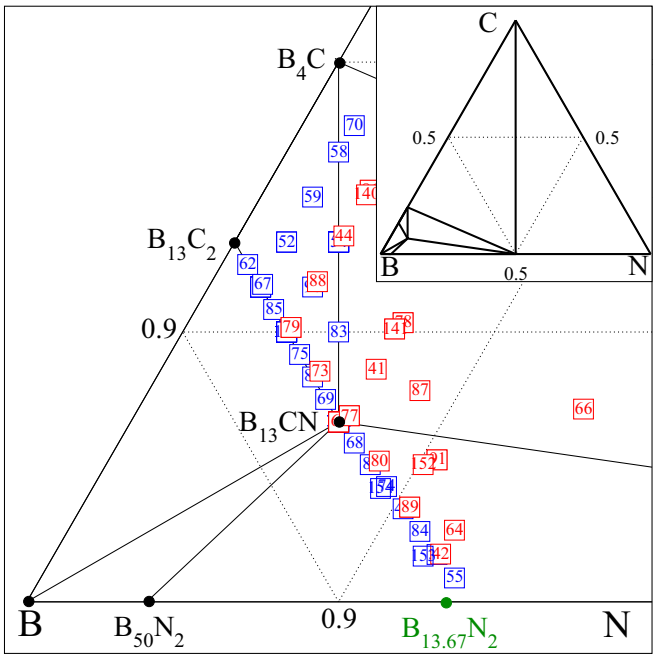

FIG. 2. Boron-rich corner of the B-C-N ternary phase diagram. Black dots show stable structures lying on vertices of the convex hull. Solid lines connecting black dots are convex hull edges. The green circle marks $B_{12.67}N_2$ (i.e., $B_{12}{\cdot}NB_{0.67}N$), which lies above the convex hull. Squares indicate ternary structures with enthalpies above the convex hull by $0 < \Delta\Delta H < 20$ meV/atom (blue) and $20 < \Delta\Delta H$ meV/atom (red). Inset shows the convex hull of the complete ternary.

The bonding character of icosahedral borides was analyzed by Longuet-Higgins and Robert [53] and others [54–56]. An icosahedral cluster of 12 sp^3-type atoms has 13 intraicosahedral bonding states, 23 intraicosahedral antibonding states, and 12 states pointing radially outwards, one from each atom. Every B_{12} icosahedron provides 36 valence electrons, 26 of which occupy the 13 intraicosahedral bonding states. Ideally, 12 additional electrons would each enter into one of the 12 external bonding orbitals. Since only 10 electrons remain, we count a B_{12} icosahedron as electron deficient by 2. In boron carbide, boron subnitride, and similar structures, six of the external bonding orbitals (those on the polar sites) combine in pairs to form three intericosahedral (ii) bonds per cell. The remaining six (those on the equatorial sites) connect to chains running along the rhombohedral cell axis, creating six ic bonds. These chains potentially provide additional electrons to resolve the electron deficiency, but as illustrated in Fig. 3, this depends on the number of electrons needed for intrachain (cc) bonds.

Consider first the three-atom CBC chain that occurs in $B_{12}{\cdot}CBC$. Each C atom has four valence electrons, three of which enter into bonds with equatorial atoms of the icosahedron with the remaining electron entering a bond to the chain-center boron. The chain-center boron has three valence electrons, only two of which are needed to bond with the neighboring carbon atoms, leaving a surplus of one electron. Recalling that the icosahedron has a deficiency of 2, we see that $B_{12}{\cdot}CBC$ remains short by one electron. This is why substitution of carbon on an icosahedral site is preferred, leading to the energetically favorable electron-precise structure $B_{11}C{\cdot}CBC$ (i.e., B_4C). Alternatively, the structure $B_{12}{\cdot}NBC$ provides the needed extra electron. However, $B_{12}{\cdot}NBN$ has an excess electron that must enter an energetically costly antibonding state.

Now consider the two-atom chains such as occur in $B_{12}{\cdot}PP$. Each P has five valence electrons (shaded in dark blue). Of these five, three enter into bonds with equatorial atoms of the icosahedron and one enters into the shared PP bond, leaving a surplus of one for each P atom. The net excess of two electrons resolves the electron deficiency of the icosahedron so that $B_{12}{\cdot}PP$ is electron precise. The same is true for valence 5 arsenic in $B_{12}{\cdot}AsAs$.

Although N is also valence 5, the N atoms are too small to directly bond. Rather, each N atom places two electrons into a lone pair. We denote the structure as $B_{12}{\cdot}N\text{-}N$, where the "-" indicates the N atoms in the chain are bonded to a vacancy instead of each other. Together with the three ic bonds, all

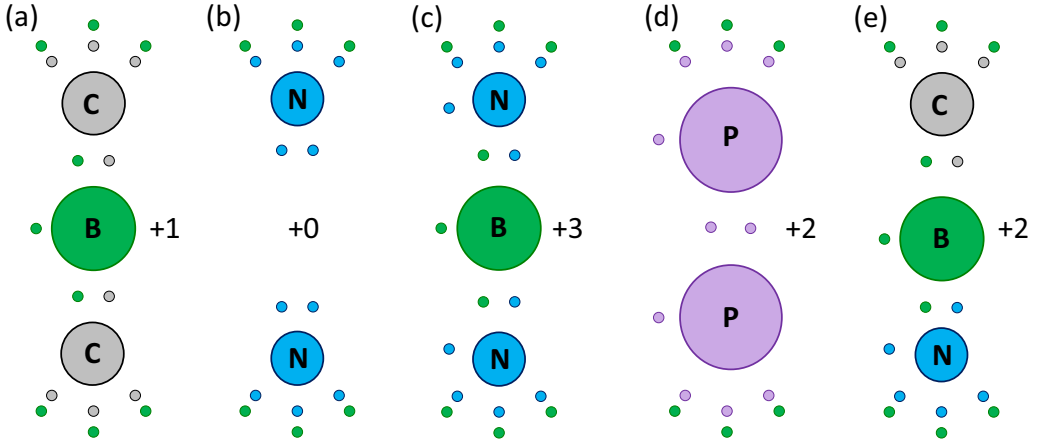

FIG. 3. Electron donation by chains. Electrons are color coded to match the atoms that donated them. The green electrons at top and bottom are donated by equatorial borons on icosahedra (not shown) that are bonded to the chain. Atomic radii and bond lengths are qualitatively accurate. (a) CBC chain donates +1, (b) unbonded N-N chain donates +0, (c) NBN chain donates +3, (d) bonded PP chain donates +2, and (e) NBC chain donates +2.

five valence electrons are utilized, so the chain provides no electrons to resolve the electron deficiency. In contrast, boron suboxide, B_{12}·O-O, is electron precise because each oxygen provides six electrons.

We are not aware of any structures containing B_{12} icosahedra with single-atom chains. Electron counting would require either a noble-gas atom or a valence 8 metal. The extreme limit, α-boron, lacks any chain at all. Here again six of the external orbitals form three ii bonds utilizing six electrons. The B_{12} icosahedron thus has $36-26-6=4$ electrons remaining, but has six external bonding orbitals unfilled. α-boron resolves this by forming a pair of two-electron three-center ($2e3c$) bonds among the six equatorial atoms, and hence is electron precise.

C. Statistical thermodynamics

Thermodynamic properties can be evaluated from the partition function

$$Z(T)=\sum_i W_i e^{-E_i/k_BT}, \tag{1}$$

where the E_i are a set of configurational energies and W_i are their multiplicities. Here we consider only discrete configurational degrees of freedom such as chemical substitution and we neglect atomic vibrations. From the partition function, we obtain the free energy $F=-k_BT\ln Z$, moments of the energy

$$\langle E^n\rangle=\frac{1}{Z}\sum_i W_i E_i^n e^{-E_i/k_BT}, \tag{2}$$

and heat capacity

$$C=(\langle E^2\rangle-\langle E\rangle^2)/k_BT^2. \tag{3}$$

The complete set of configurations distributing B, C, and N atoms on $hR15$ is too large to be thoroughly sampled. Instead we concentrate our attention on mixtures of complete intact primitive cells, so that we target likely low-energy structures. Since all these rhombohedral primitive cells are of similar sizes, we can mix different primitive cells to construct larger supercells with new stoichiometries. By mixing multiple types of primitive cells, we can make an electron-precise supercell from primitive cells which are not electron precise. For example, we construct a $B_{38}N_6$ supercell from two $B_{13}N_2$ and one $B_{12}N_2$, and this electron-precise structure turns out to be more stable than either primitive cell alone.

Our mixture method generates a small subset of all the possible structures. We consider all possible chain disorder, but neglect disorder of polar carbons [19] in $B_{11}C$ icosahedra. Thus only a limited set of structures are studied, but these are all from a consistent family and we expect the entropies of the polar carbons will approximately cancel out of relative free energies of differing chain types.

III. RESULTS

We present our results first for the individual binary combinations B-C, B-N, and C-N, followed by the ternary B-C-N. Our discussion of the ternary begins with the line connecting pure carbon to equiatomic boron nitride. Structures along this line include the isostructural diamond/c-BN and the stacked 2D honeycomb graphite/h-BN. We then turn to our main result, with predicted stability of the electron precise structure B_{12}·NBC followed by pseudobinary combinations of B_{12}·NBC with certain B-C and B-N binaries. Finally, we present complete solid-state phase diagrams for the B-rich ternary at various temperatures.

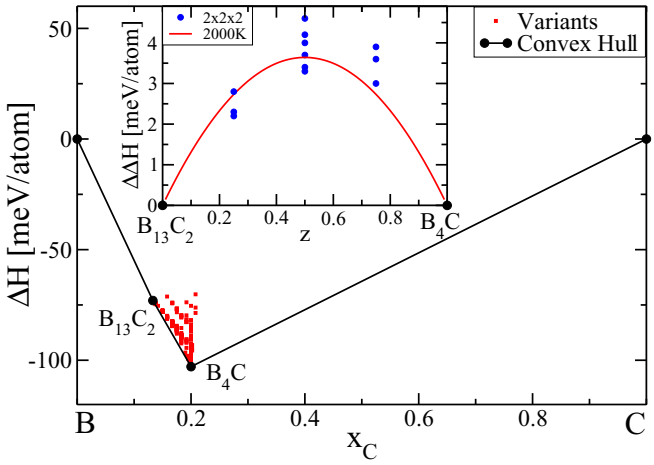

FIG. 4. Enthalpies of B-C showing the $B_{13}C_2$ and B_4C structures on the convex hull and a scatter plot of higher enthalpy structures. Inset shows the region $B_{13}C_2$ to B_4C with structures restricted to CBC chains and a single choice of polar carbon site. $\Delta\Delta H$ is enthalpy relative to the tie line joining competing compounds. The red line is the parabolic approximation to $\langle E\rangle$ at $T=2000$ K.

A. B-C

Two structures lie on the convex hull of the alloy system B-C [19]: electron-deficient $B_{13}C_2$ in the form of B_{12}·CBC, with rhombohedral symmetry, marginally touches the hull; and electron-precise B_4C in the form of $B_{11}C$·CBC, with monoclinic symmetry, provides a strong sharp enthalpy minimum. At elevated temperatures, $B_{13}C_2$ extends to cover a broad concentration range, while B_4C undergoes an orientational order-disorder transition to this disordered rhombohedral state.

Figure 4 illustrates the enthalpies of these structures and many variants that differ in the specific placements of B and C atoms among the 15 atomic sites per cell. The inset shows relative enthalpies of a subset of structures over the composition range between the two low-temperature stable phases. In the inset, we only consider structures with CBC chains (i.e., no BBC or other chain types), and only B_{12} or $B_{11}C$ icosahedra in a $2\times2\times2$ supercell. Furthermore, in the $B_{11}C$ icosahedra, the carbon always occupies the same polar site. In other words, each structure is a mixture of perfect B_{12}·CBC cells and identically aligned $B_{11}C$·CBC cells. We neglect orientational disorder because we wish to focus on compositional effects. Orientational effects have been previously analyzed [19,20] and would have a quantitative but not qualitative impact on our further discussion. Our present study yields a temperature-dependent solubility range between $B_{13}C_2$ and B_4C.

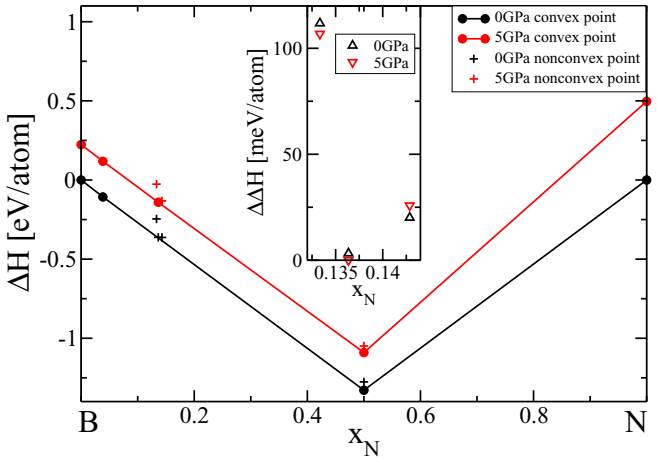

FIG. 5. Convex hull, enthalpy of BN binary at $P = 0$ and 5 Gpa. Vertices of the convex hull are highlighted as solid dots. The inset shows $\Delta\Delta$H for rhombohedral structures with stoichiometry $B_{13}N_2$, $B_{12.67}N_2$, and $B_{12}N_2$, from left to right, respectively.

B. B-N

We calculate enthalpies of B-N at P = 0 and 5GPa, as shown in Fig. 5. At pressure $P = 0$, we find just a single convex hull vertex corresponding to h-BN, consistent with the assessed phase diagram. At high pressure, $P = 5$ GPa, c-BN has lower enthalpy than h-BN owing to its much lower atomic volume. Also, a second vertex appears, corresponding to a supercell of B_{12}·NBN with a specific pattern of chain B vacancies. This is nearly consistent with a recent report claiming high-pressure stability of the same structure but with full chain occupancy [4,25]. The inset shows enthalpies relative to competing phases over a small range, from the electron-rich B_{12}·NBN to the electron-poor B_{12}·N-N. Only the electron-precise B_{12}·$NB_{0.67}N$ touches the convex hull. This structure consists of a supercell in which complete NBN chains mix with chain boron vacancies in a 2:1 ratio. The enthalpy minimizing structure maximizes the separation of the chain boron vacancies. We also considered a large number of alternate structures including some with N atoms locating on the icosahedra, and found these configurations were not stable.

C. C-N

For C-N binaries, $P = 0$ calculations find that all of the tested structures are quite high in energy ($\gtrsim$100 meV/atom), including various C_3N_4 and $C_{11}N_4$ structures [27,28]. This confirms the thermodynamic metastability of C-N binaries.

D. C-BN line

To resolve the conflict over the nature of sp^2-bonded layered B-C-N compounds [39,42], we created structures along the C-h-BN line by replacing C in graphite with B or N, or C_2 with BN, and similarly by replacing B, N, and BN in h-BN with C or C_2. All possible arrangements in $2 \times 2 \times 1$ supercells have been calculated and none of them is energetically stable at $P = 0$, with energy cost at least $\Delta E >$ 1.0 eV/defect. Even allowing for configurational entropy, the energy cost is so high that the mutual solubility is low, supporting the reported separation into domains of h-BN and C (graphene) in 2D atomic films [39]. Stacking of alternating 2D layers of C and h-BN, as in 2D heterostructures [9], has a low cost in energy (4–8 meV/atom depending on stacking registry) but the entropy is subextensive (i.e., entropy per atom vanishes in the limit of infinite system size), so even these structures will not occur in equilibrium. A similar study of sp^3-bonded cubic solids likewise obtains high energies with $\Delta\Delta H > 250$ meV/atom, suggesting phase separation in equilibrium at $P = 0$.

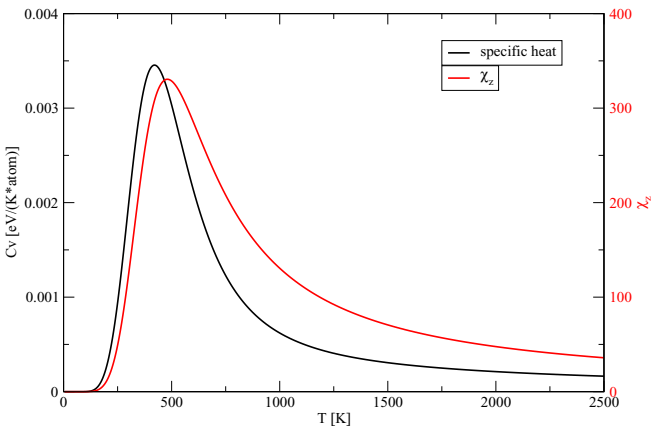

FIG. 6. Heat capacity C and susceptibility χ_z of B_{12}·NBC, evaluated in a $2 \times 2 \times 2$ supercell.

E. B_{12}·NBC

Since B_{12}·CBC is deficient by one electron, it is natural to replace one C with N, yielding the electron-precise B_{12}·NBC. We find the enthalpy of this structure lies 35 meV/atom below the tie plane of competing structures. Consequently, it occupies a vertex of the convex hull as illustrated in Fig. 2, implying stability down to low temperatures. As an electron-precise compound, it is expected to be semiconducting, with a band gap predicted by DFT to be 2.5 eV (3.3 eV using the hybrid functional HSE06 [57] with range separation parameter 0.2). Additionally, because of the symmetry breaking of the NBC chain, it has a net polarization P_z. The space group is $R3m$ as opposed to group $R\bar{3}m$ of B_{12}·CBC.

The NBC chain orientation introduces an Ising-like degree of freedom (NBC vs CBN). To investigate the chain ordering as a function of temperature, we use the independent cell approximation [58] and enumerate all $2^8 = 256$ chain configurations in a $2 \times 2 \times 2$ supercell, obtaining 14 symmetry-inequivalent structures and their multiplicities. We then sum up the partition function according to Eq. (1), obtaining other thermodynamic quantities including the free energy $F(T)$ and the entropy $S(T)$. Figure 6 plots the heat capacity C [Eq. (3)] and the dielectric susceptibility

$$\chi_z = \frac{\langle P_z^2 \rangle - \langle P_z \rangle^2}{k_B T}. \quad (4)$$

The peaks imply that an order-disorder transition occurs in the vicinity of $T = 500$ K. The peaks are broadened by the finite cell size of the independent cell approximation.

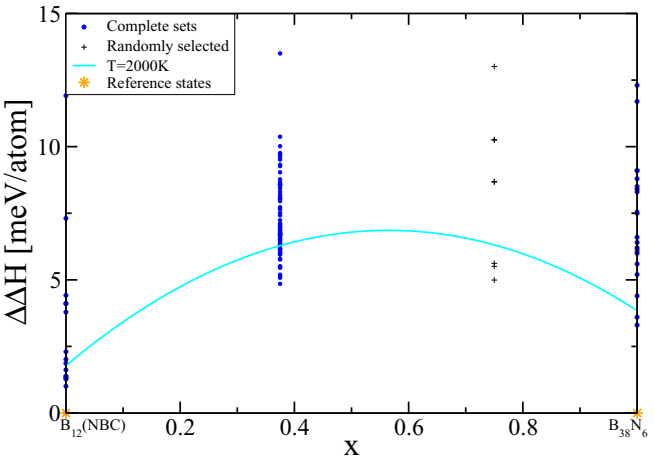

FIG. 7. Relative enthalpies $\Delta\Delta H$ along line B_{12}·NBC-$B_{38}N_6$. Points are calculated supercell structures; stars are reference (convex hull) states. Curve is $\Delta\Delta H$ derived from Eq. (2) at $T = 2000$ K.

F. B_{12}·NBC-$B_{38}N_6$ line

We now consider the line connecting electron-precise structures B_{12}·NBC and B_{12}·$NB_{0.67}N$, anticipating these will have energies lower than compounds lying off this line. These structures are mixtures of three types of primitive cells: B_{12}·NBC, B_{12}·NBN, and B_{12}·N-N, with a fixed ratio between B_{12}·NBN and B_{12}·N-N of 2:1. We now formulate a free-energy model to investigate the mutual solubility of these cell types.

Modeling the free energy $G = H - TS$ requires estimating both the enthalpy and the entropy as functions both of composition and temperature. We first address the enthalpy, which we shall measure relative to competing ground states, defining $\Delta\Delta H$. In the present case, the competing structures are the ternary ground state B_{12}·NBC, and the binary of composition $B_{12.67}N_2$. However, as shown in Fig. 5, the ground state at this composition is a mixture of two competing binaries, $B_{50}C_2$, and h-BN, so we take the tie-line enthalpy as our reference. We formed $2 \times 2 \times 2$ supercells containing a fraction x of $NB_{0.67}N$ chains and a fraction $1 - x$ of NBC chains. Individual energies are given in Fig. 7. Using the statistical mechanics formulation in Eq. (2), we can evaluate the temperature-dependent mean enthalpy $\Delta\Delta H(x,T)$ at $x = 0, 1/3$ and $x = 1$. We fit these to a quadratic function of x,

$$E(x,T) = u(T)x^2 + v(T)x + w(T), \tag{5}$$

yielding temperature-dependent coefficients $u(T)$, $v(T)$, and $w(T)$. As a test of our fit, we compare the parabola with randomly selected $\Delta\Delta H$ values at $x = 2/3$. The $2 \times 2 \times 2$ supercell contains too many structures at $x = 2/3$ to apply the statistical mechanical method as we did at the other values of x.

Next we derive an ideal solution expression for entropy. If there are N primitive cells and the composition ratio of mixture is x, the number of B_{12}·NBN primitive cells is $\frac{2}{3}Nx$, the number of B_{12}·N-N primitive cells is $\frac{1}{3}Nx$, and the number of B_{12}·NBC primitive cells is $N(1-x)$. Randomly mixing the three components together, the entropy per atom is

$$S = \frac{k_B}{15 - \frac{x}{3}}\left\{ -(1-x)\ln(1-x) - \frac{x}{3}\ln\frac{x}{3} - \frac{2x}{3}\ln\frac{2x}{3} + (1-x)\ln\Omega_0 \right\}. \tag{6}$$

Here, $\Omega_0 = \Omega_0(T) = e^{S_0(T)/k_B}$ represents the number of microstates per B_{12}·NBC primitive cell arising from the NBC chain orientations and S_0 is entropy per B_{12}·NBC primitive cell obtained through the partition function approach, as described in Sec. III E.

Free-energy curves at various temperatures are shown in Fig. 8(a). Lack of convexity at low temperatures produces miscibility gaps that we determine via the double-tangent construction. Below $T = 847$ K, the convex hull consists of a narrow interval of stable ternary close to $x = 0$, then jumps to the B-N binary ground state. Above $T = 847$ K, a second interval of stable ternary opens close to $x = 1$. At $T = 920$ K, $\Delta\Delta G$ vanishes at $x = 1$, and the second interval of stable ternary extends all the way to $x = 1$. Finally, at $T = 1355$ K, $\Delta\Delta G$ becomes fully convex, and the ternary extends over the

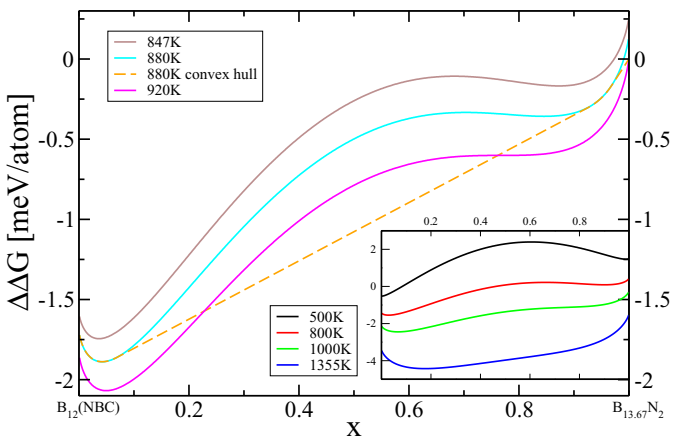

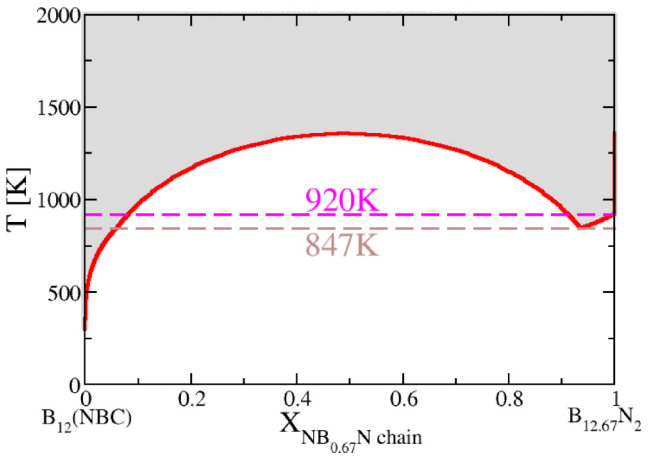

FIG. 8. (a) Free-energy curves over narrow temperature range with two miscibility ranges. Orange dashed line shows the convex hull for $T = 880$ K. Inset shows free-energy curves over broad temperature range from low to complete miscibility. (b) Vertical section with temperature-dependent solubility region shaded.

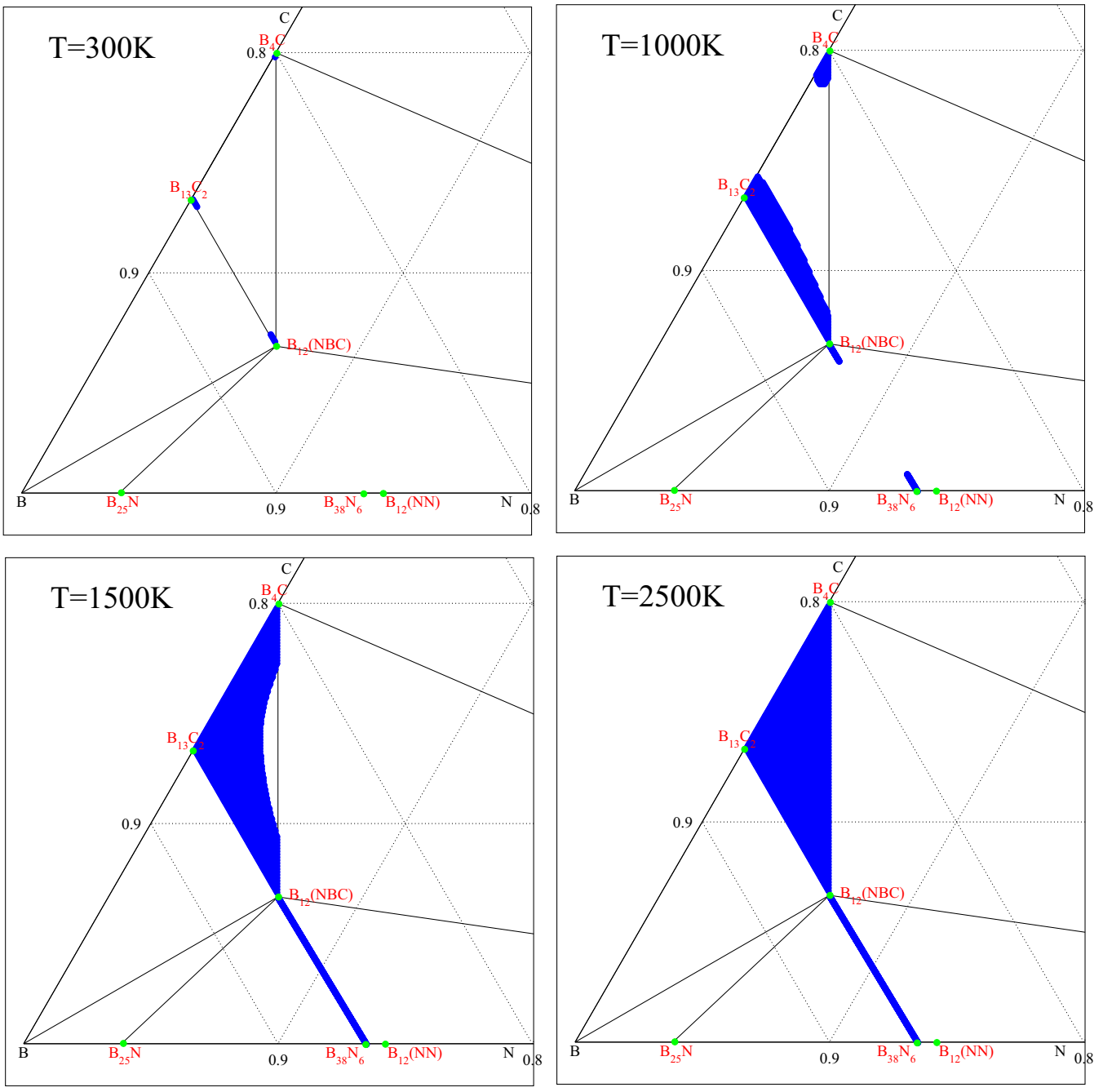

FIG. 9. Solubility range (shown as blue) at $T = 300$ K (top left), $T = 1000$ K (top right), $T = 1500$ K (bottom left), and $T = 2500$ K (bottom right).

entire interval $x = 0$ to $x = 1$. Figure 8(b) shows a predicted vertical section of the ternary diagram along this line.

G. B_4C-$B_{13}C_2$-B_{12}·NBC triangle

From Fig. 2, we see that there are many structures in the triangle extending from binary boron carbide to the stable ternary B_{12}·NBC with $0 < \Delta\Delta H < 20$ meV/atom, so we expect some solubility of nitrogen into boron carbide at elevated temperatures. To explore this possibility, we need a free-energy model for the region. Although the ternary composition space is two dimensional, we introduce three composition variables. We define x as the fraction of B_{12}·CBC, y as the fraction of B_{12}·NBC, and $z = 1 - x - y$ as the fraction of $B_{11}C$·CBC. Our goal is to model the free energy $F(x,y,z;T)$ over the triangle whose vertices are $(x,y,z) = (1,0,0)$, $(0,1,0)$, and $(0,0,1)$.

First consider the enthalpy $\Delta\Delta H(x,y,z;T)$. As in the previous section, we model it as a quadratic function. Support for this comes from the enthalpies of boron carbide (i.e., the triangle edge B_{12}·CBC-$B_{11}C$·CBC) previously shown in Fig. 4, and the other two additional edges (i.e., B_{12}·CBC-B_{12}·NBC and $B_{11}C$·CBC-B_{12}·NBC, not shown). Because the three composition variables obey a linear relationship, we may

suppress the variable z and keep only terms involving x and y. A quadratic of two variables contains six terms and requires six data points to determine it. We take these data points as the three reference values at the triangle vertices, and the three values at the edge midpoints. Values at the edge midpoints come from our partition function approach as previously.

Now consider the entropy $S(x,y,z;T)$. Including the entropy of NBC chain orientation and mixing of chain types within the ideal solution model, the entropy per cell is

$$S(x,y,z)/k_B = -x\ln x - y\ln y - z\ln z + y\ln\Omega_0. \quad (7)$$

Given the free energy per atom inside the $B_{13}C_2$-B_4C-B_{12}·NBC triangle region, we determine the solubility ranges as functions of temperature, as illustrated in Fig. 9. Blue points show solubility ranges and the empty regions reveal miscibility gaps. Note that the miscibility gap within the B-C binary persists to temperatures above 1000 K, contrary to an earlier more accurate estimate of miscibility above 600 K [16], because here we neglect the configurational entropy of polar carbons. Miscibility is complete throughout the entire triangle above 2423 K.

IV. CONCLUSIONS

We explore the B-C-N solid-state ternary phase diagram using first-principles total-energy calculations coupled with statistical mechanics. A number of plausible approximations are made to simplify the task: vibrational free energies are neglected as these will nearly cancel among similar structures at different compositions; disorder of polar carbons is neglected, again assuming approximate cancellation; free energies are constructed in the spirit of regular solution models, with quadratic composition dependence of enthalpies and ideal entropies of mixing. Neglect of polar carbon disorder and BBC chains causes us to significantly underestimate the composition width of the rhombohedral boron carbide phase.

The striking result is our prediction of an ordered ternary $B_{13}CN$ similar in structure to boron carbide with B_{12} icosahedra and NBC chains that is predicted to be stable at all temperatures below melting. At elevated temperatures, this structure joins into a solid solution that covers a triangular area within the ternary phase diagram extending to binary boron carbide, and along a line extending to boron subnitride. Additionally, we refine the stoichiometry of boron subnitride, proposing an ideal composition of $B_{12.67}N_2$. That is, B_{12} icosahedra with a 2:1 mixture of NBN and N-N chains.

Our search for stable layered 2D ternaries and ultrahard ternaries was unsuccessful, as the predicted energy costs of chemical substitution proved prohibitive in thermal equilibrium at ambient pressures.

ACKNOWLEDGMENTS

We thank Antoine Jay and Nathalie Vast for discussions on the variety of boron carbide chain types and Will Huhn for collaborations on binary boron carbide. This work was supported in part by the U.S. Department of Energy Grant No. DE-SC0014506. H.Z. acknowledges support through the Yan Jici Talent Students Program in Physics, University of Science and Technology of China.

[1] T. Ogitsu, E. Schwegler, and G. Galli, Chem. Rev. **113**, 3425 (2013).
[2] A. R. Oganov, J. Chen, C. Gatti, Y. Ma, Y. Ma, C. W. Glass, Z. Liu, T. Yu, O. O. Kurakevych, and V. L. Solozhenko, Nature (London) **457**, 863 (2009).
[3] M. A. White, A. B. Cerqueira, C. A. Whitman, M. B. Johnson, and T. Ogitsu, Angew. Chem. **127**, 3697 (2015).
[4] O. O. Kurakevych and V. L. Solozhenko, Acta Crystallogr. Sec. C **63**, i80 (2007).
[5] F. Bundy, H. Hall, H. Strong, and R. Wentorf, Nature (London) **176**, 51 (1955).
[6] R. Wentorf Jr., J. Chem. Phys. **34**, 809 (1961).
[7] S. Veprek, A. Zeer, and R. Riedel, *Handbook of Ceramic Hard Materials* (Wiley, Weinheim, Germany, 2000).
[8] J. Haines, J. Leger, and G. Bocquillon, Annu. Rev. Mater. Res. **31**, 1 (2001).
[9] A. K. Geim and I. V. Grigorieva, Nature (London) **499**, 419 (2013).
[10] M. Widom and M. Mihalkovič, Phys. Rev. B **77**, 064113 (2008).
[11] K. A. Schwetz and P. Karduck, J. Less-Common Met. **175**, 1 (1991).
[12] R. Schmechel and H. Werheit, J. Solid State Chem. **154**, 61 (2000).
[13] E. Betranhandy, N. Vast, and J. Sjakste, Solid State Sci. **14**, 1683 (2012).
[14] K. Shirai, K. Sakuma, and N. Uemura, Phys. Rev. B **90**, 064109 (2014).
[15] A. Ektarawong, S. I. Simak, L. Hultman, J. Birch, and B. Alling, Phys. Rev. B **92**, 014202 (2015).
[16] W. P. Huhn and M. Widom, J. Stat. Phys. **150**, 432 (2012).
[17] D. M. Bylander and L. Kleinman, Phys. Rev. B **43**, 1487 (1991).
[18] N. Vast, J. Sjakste, and E. Betranhandy, J. Phys.: Conf. Ser. **176**, 012002 (2009).
[19] M. Widom and W. P. Huhn, Solid State Sci. **14**, 1648 (2012).
[20] S. Yao, W. Huhn, and M. Widom, Solid State Sci. **47**, 21 (2015).
[21] A. Jay, N. Vast, J. Sjakste, and O. H. Duparc, Appl. Phys. Lett. **105**, 031914 (2014).
[22] H. Okamoto, J. Phase. Equil. **21**, 208 (2000).
[23] H. J. Seifert and F. Aldinger, *High Performance Non-oxide Ceramics* (Springer, New York, 2002), pp. 1–58.
[24] R. S. Pease, Acta Cryst. **5**, 356 (1952).
[25] V. L. Solozhenko, O. O. Kurakevych, V. Z. Turkevich, and D. V. Turkevich, J. Phys. Chem. **114**, 5819 (2010).
[26] V. L. Solozhenko and O. O. Kurakevych, J. Phys.: Conf. Ser. **121**, 062001 (2008).
[27] D. Zhogolev, O. Bugaets, and I. Marushko, J. Struct. Chem. **22**, 33 (1981).
[28] M. L. Cohen, Phys. Rev. B **32**, 7988 (1985).
[29] A. Y. Liu and R. M. Wentzcovitch, Phys. Rev. B **50**, 10362 (1994).

[30] D. M. Teter and R. J. Hemley, Science **271**, 53 (1996).
[31] L. W. Yin, M. S. Li, Y. X. Liu, J. L. Sui, and J. M. Wang, J. Phys. Condens. Matter **15**, 309 (2003).
[32] G. Algara-Siller, N. Severin, S. Y. Chong, T. Björkman, R. G. Palgrave, A. Laybourn, M. Antonietti, Y. Z. Khimyak, A. V. Krasheninnikov, J. P. Rabe *et al.*, Angew. Chem. **126**, 7580 (2014).
[33] V. Tomashik *et al.*, in *Refractory Metal Systems* (Springer, New York, 2009), pp. 444–473.
[34] H. Sun, S.-H. Jhi, D. Roundy, M. L. Cohen, and S. G. Louie, Phys. Rev. B **64**, 094108 (2001).
[35] M. Mattesini and S. Matar, Intl. J. Inorgan. Mater. **3**, 943 (2001).
[36] Q. Li, D. Zhou, H. Wang, W. Chen, B. Wu, Z. Wu, and W. Zheng, Solid State Commun. **152**, 71 (2012).
[37] V. L. Solozhenko, D. Andrault, G. Fiquet, M. Mezouar, and D. C. Rubie, Appl. Phys. Lett. **78**, 1385 (2001).
[38] Y. Zhao, D. He, L. Daemen, T. Shen, R. Schwarz, Y. Zhu, D. Bish, J. Huang, J. Zhang, G. Shen *et al.*, J. Mater. Res. **17**, 3139 (2002).
[39] L. Ci, L. Song, C. Jin, D. Jariwala, D. Wu, Y. Li, A. Srivastava, Z. Wang, K. Storr, L. Balicas *et al.*, Nat. Mater. **9**, 430 (2010).
[40] X. Wei, M.-S. Wang, Y. Bando, and D. Golberg, ACS Nano **5**, 2916 (2011).
[41] W.-Q. Han, H.-G. Yu, and Z. Liu, Appl. Phys. Lett. **98**, 203112 (2011).
[42] W. Lei, S. Qin, D. Liu, D. Portehault, Z. Liu, and Y. Chen, Chem. Commun. **49**, 352 (2013).
[43] D. P. Gopalan, P. C. Mende, S. C. de la Barrera, S. Dhingra, J. Li, K. Zhang, N. A. Simonson, J. A. Robinson, N. Lu, Q. Wang *et al.*, arXiv:1509.04531 [J. Mater. Res (to be published)].
[44] K. Yuge, Phys. Rev. B **79**, 144109 (2009).
[45] C. Özdoğan, J. Kunstmann, and A. Quandt, Philos. Mag. **94**, 1841 (2014).
[46] G. Kresse and J. Hafner, Phys. Rev. B **47**, 558 (1993).
[47] G. Kresse and J. Hafner, Phys. Rev. B **49**, 14251 (1994).
[48] G. Kresse and J. Furthmüller, Phys. Rev. B **54**, 11169 (1996).
[49] G. Kresse and J. Furthmüller, Comput. Mater. Sci. **6**, 15 (1996).
[50] P. E. Blöchl, Phys. Rev. B **50**, 17953 (1994).
[51] G. Kresse and D. Joubert, Phys. Rev. B **59**, 1758 (1999).
[52] J. P. Perdew, K. Burke, and M. Ernzerhof, Phys. Rev. Lett. **77**, 3865 (1996).
[53] H. Longuet-Higgins and M. d. V. Roberts, Proc. R. Soc. London A **230**, 110 (1955).
[54] R. Hoffmann and W. N. Lipscomb, J. Chem. Phys. **36**, 2179 (1962).
[55] W. N. Lipscomb, J. Less-Common Met. **82**, 1 (1981).
[56] M. M. Balakrishnarajan, P. D. Pancharatna, and R. Hoffmann, New J. Chem. **31**, 473 (2007).
[57] J. Heyd, G. E. Scuseria, and M. Ernzerhof, J. Chem. Phys. **124**, 219906 (2006).
[58] G. S. Pomrehn, E. S. Toberer, G. J. Snyder, and A. van de Walle, Phys. Rev. B **83**, 094106 (2011).